



On the numerical simulation of two-phase flow in shale gas reservoirs

Gillyan Macário da Silva¹, Mayksoel Medeiros de Freitas¹, Grazione de Souza¹, Helio Pedro Amaral Souto¹

¹*Polytechnic Institute, Rio de Janeiro State University*

Bonfim Street 25th, 28.625-570, Nova Friburgo, Rio de Janeiro, Brazil

gillyan.silva@iprj.uerj.br; mayksoel@iprj.uerj.br; gsouza@iprj.uerj.br; helio@iprj.uerj.br

Abstract. In this paper, we carry out numerical simulations of isothermal two-phase gas-water flow in shale gas reservoirs. We considered the effects of slippage and adsorption employing the Klinkenberg model and the Langmuir isotherm for the gas phase. It also incorporates a pressure-dependent correction in determining effective permeability for both phases and horizontal wells for production. The Control Volume-Finite Difference method is applied to discretize the governing flow equations, employing centered block grids and fully implicit numerical formulations. We linearize the discretized equation for gas phase pressure using the Picard method, while we use the Newton method for the discretized equation for water phase saturation. The results are analyzed in terms of the pressure at the production well, leading to an evaluation of how the effects considered for the effective permeabilities of the phases influence pressure variation and the times of occurrence of the flow regimes for the considered well-reservoir system.

Keywords: horizontal well, Picard-Newton method, shale gas, two-phase flow.

1 Introduction

According to Al-Twajri et al. [1], the increasing energy demand has led to the exploration and production of unconventional sources of oil and gas. Shale gas reservoirs, for example, are one of the principal unconventional resources. In these reservoirs, advances in horizontal drilling and hydraulic fracturing techniques have been essential to achieving economically viable production rates. In addition to their ultra-low absolute permeability, we can characterize shale gas reservoirs by complex gas transport mechanisms and geometries of natural and hydraulic fractures. Still, according to Al-Twajri et al. [1], production from shale gas reservoirs is predominantly composed of a two-phase flow of gas and water, and in the work mentioned above, the authors considered two-phase flow in shale gas reservoirs, including the presence of fractures, highlighting their function in the recovery of gas and water from the reservoir. The initial water saturation was one of the parameters evaluated.

Shale gas reservoirs are known for their low porosity and low absolute permeability of the matrix and often present heterogeneity due to natural fractures. If we use hydraulic fracturing, the fluid can invade the reservoir, resulting in low efficiency. According to Xu et al. [2], numerical methods can present convergence problems when studying cases of two-phase flow gas-water in shale gas reservoirs. In this context, the authors used fractal theory to quantitatively characterize hydraulic fractures in multifractured horizontal wells and the two-phase flow of gas-water in shale reservoirs. They used the Meshless Weighted Least-squares (MWLS) method in the simulations. The results were consistent with the solutions obtained with the Finite Difference Method (FDM). However, the new approach had a lower computational cost. Also, considering the obtained results, the higher the initial water saturation, the higher the resistance to the flow of the gas phase, and when the spacing between the fractures decreases, the daily gas production increases.

In fact, several mechanisms can be considered in the physical-mathematical modeling in order to discuss low water recovery during the production period of a shale gas reservoir, such as water present in the fracture network, water imbibition related to osmotic pressure, and capillary pressure. These factors hinder the flow of water, which can be described by a modified Darcy's law for cases of low velocities, as discussed by He et al. [3]. In this article, the authors used a modified Darcy's law for low-velocity cases to describe water transport and another modified

Darcy's law considering slip and free molecular flow mechanisms for gas transport in a shale gas reservoir. The authors performed a sensitivity study using numerical simulations to discuss water recovery in shale formations.

Zhang and Yang [4] studied numerically the two-phase water-gas flow in a shale gas reservoir being produced by a multi-fractured horizontal. The authors considered non-Darcy inertial flow and slippage, with an iterative method applied to update the gas/water saturation in each fracture segment within discrete fracture networks. A skin factor was defined in the fracture and used to represent the change in relative permeability in the matrix at each time step. Besides, adsorption is incorporated into the diffusivity equation to accurately predict shale gas production considering the gas adsorbed in nanoscale porous media. According to the authors, desorption in the matrix subsystem can increase gas production but decrease water production. Compared to the gas/water production rates observed in field applications, the solutions obtained with the method were compatible.

In the paper by Zhang et al. [5], a model for production prediction for multi-stage fractured horizontal wells in shale gas reservoirs is proposed based on the Multiple Interacting Continuum (MINC) theory (considering organic/inorganic matrix, natural fracture system) and the lower-dimensional discrete fracture network (DFN) models (for hydraulic fracture system) which describe the unconventional flow mechanisms in the shale system, such as non-Darcy multiscale flow in an ultrathin matrix, ad-desorption at the surface of organic materials, rock deconsolidation in natural fractures, high-velocity turbulent flow near the wellbore, and multiphase behaviors. Zhang et al. [5] also proposed a new hybrid method of Control Volume Finite Element (CVFE) and Finite Difference (FD) to obtain the numerical results. The authors validated the accuracy of the results, and sensitivity analysis of some factors, for example, permeability and Langmuir volume, is performed to assess the impacts on production performance.

Concluding, we can say that shale gas reservoirs typically contain significant volumes of gas, but their low intrinsic permeability is a drawback. Indeed, technological advances using horizontal well drilling have led to economically viable production from such reservoirs, and in this context, numerical simulations are relevant in planning natural gas recovery. In this work, we performed numerical simulations for horizontal well production in a shale gas reservoir considering the isothermal two-phase water/gas flow, including slippage, a stress correction for matrix permeability, and natural gas adsorption.

2 Porous media two-phase flow modeling

We consider the mass balances for the water and gas phases [6], respectively,

$$\frac{\partial}{\partial t} \left(\frac{\phi S_w}{B_w} \right) + \nabla \cdot \left(\frac{\mathbf{v}_w}{B_w} \right) - \dot{q}_{scw} = 0, \quad (1)$$

$$\frac{\partial}{\partial t} \left(\frac{\phi S_g}{B_g} \right) + \frac{\partial}{\partial t} \left(\frac{\rho_s V_{ads}}{B_g} \right) + \nabla \cdot \left(\frac{\mathbf{v}_g}{B_g} \right) - \dot{q}_{scg} = 0, \quad (2)$$

where, for $\alpha = w, g$ (w for water and g for gas), \mathbf{v}_α is the apparent phase velocity, B_α is the formation-volume-factor, ϕ the porosity, S_α the phase saturation, $\dot{q}_{m\alpha}$ is a source term, ρ_s the rock density, and V_{ads} is adsorption gas volume.

For the momentum balance, we have respectively for water and gas phases [6]

$$\mathbf{v}_w = -\frac{\mathbf{k}_{aw} k_{rw}}{\mu_w} \left(\nabla p_w - \frac{\rho_{scw} g}{B_w} \nabla D \right), \quad (3)$$

$$\mathbf{v}_g = -\frac{\mathbf{k}_{ag} k_{rg}}{\mu_g} \left(\nabla p_g - \frac{\rho_{scg} g}{B_g} \nabla D \right), \quad (4)$$

where \mathbf{k}_{aw} is the apparent permeability tensor for water, \mathbf{k}_{ag} is the apparent permeability tensor for gas, $k_{r\alpha}$ the relative permeability, μ_α the fluid viscosity, p_α the pressure, D the depth, $\rho_{sc\alpha}$ the fluid density in standard conditions, and g is the gravity acceleration magnitude. The apparent permeability tensors for the water and gas phases are determined using [4]

$$\mathbf{k}_{aw} = e^{-\gamma(p_0-p)} \mathbf{k}, \quad (5)$$

$$\mathbf{k}_{ag} = e^{-\gamma(p_0-p)} \left(1 + \frac{b}{p} \right) \mathbf{k}, \quad (6)$$

where \mathbf{k} is the absolute permeability tensor, γ is a coefficient related to stress changes for the apparent permeability, p_0 is a reference pressure, and b is the Klinkenberg factor, incorporating, therefore, the slippage [4].

For the gas adsorption, we employed Langmuir's isotherm $V_{ads} = V_L \left(\frac{p}{p + p_L} \right)$, where V_L and p_L are the Langmuir volume and pressure, respectively. Considering fully saturated porous media and capillary effect, we have $S_w + S_g = 1$ and for a two-phase flow $p_c = p_g - p_w$, where p_c is the capillary pressure.

Introducing Eqs. (3) and (4) in Eqs. (1) and (2), we obtain

$$\nabla \cdot \left[\frac{k_{rg}}{\mu_g B_g} \mathbf{k}_{ag} \left(\nabla p_g - \frac{\rho_{scg} g}{B_g} \nabla D \right) \right] = \frac{\partial}{\partial t} \left[\frac{\phi(1 - S_w)}{B_g} \right] + \frac{\partial}{\partial t} \left(\frac{\rho_s V_{ads}}{B_g} \right) - \dot{q}_{scg}, \quad (7)$$

$$\nabla \cdot \left[\frac{k_{rw}}{\mu_w B_w} \mathbf{k}_{aw} \left(\nabla p_g - \frac{dp_c}{dS_w} \nabla S_w - \frac{\rho_{scg} w}{B_w} \nabla D \right) \right] = \frac{\partial}{\partial t} \left(\frac{\phi S_w}{B_w} \right) - \dot{q}_{scw}, \quad (8)$$

where we applied the chain rule on the capillary term and assumed a saturated porous media.

We impose initial conditions in the form $p_g(x, y, z, t_0) = p_{init}(x, y, z)$ and $S_w(x, y, z, t_0) = S_{init}(x, y, z)$, where p_{init} and S_w are the initial gas pressure and water saturation values, respectively. About the boundary conditions, we adopted no-flow conditions at the outer boundaries of the reservoir. We determined fluid and rock properties according to Freitas [7]. The Formation-Volume-Factor (FVF) of water and gas can be expressed as the ratio between the volume of water or gas at reservoir conditions and its volume at standard surface conditions. The FVF for the water and gas phases are determined using, respectively [8],

$$B_w = \frac{B_{w,sc}}{1 + c_w (p_w - p_{sc})}, \quad (9)$$

$$B_g = \frac{p_{sc} Z T}{T_{sc} p_g}, \quad (10)$$

where $B_{w,sc}$, p_{sc} , T_{sc} , c_w , Z , T are, respectively, the water FVF in standard conditions, the standard condition pressure, the standard condition temperature, the water compressibility, the real gas compressibility factor and the reservoir temperature.

The gas compressibility, c_g , is determined using [6],

$$c_g = \frac{1}{p_g} - \frac{1}{Z} \left. \frac{\partial Z}{\partial p_g} \right|_T. \quad (11)$$

In this work, the capillary pressure is computed using power-law models [7], as

$$p_c(S_w) = p_{c,max} \left(\frac{1 - S_w - S_{gc}}{1 - S_{iw} - S_{gc}} \right)^{epc}, \quad (12)$$

where S_{iw} , S_{gc} , $p_{c,max}$ and epc are, respectively, the irreducible water saturation, the critical gas saturation, a maximum value for capillary pressure and a coefficient of the model.

3 Numerical solution

We discretize the domain of dimensions L_x , L_y , and L_z into n_x , n_y , and n_z in the x -, y -, and z -directions, respectively. The indices i , j , and k indicate the blocks in the x -, y -, and z -directions, respectively. In this system, we reference block boundaries using the notation $i + 1/2$, j , k , e.g., for the boundary common to cells i , j , k and $i + 1$, j , k . Similarly, we indicate the faces of the cells in the other spatial directions. We start the discretization of Eqs. (7) and (8) by integrating them over a control volume (Figure 1) and, subsequently, by integrating over time from t^n to $t^{n+1} = t^n + \Delta t$, where Δt is the time increment.

We use a notation [7] in which we identify the faces of finite volumes by lowercase letters: $(i - 1/2, j, k) = w$, $(i + 1/2, j, k) = e$, $(i, j - 1/2, k) = n$, $(i, j + 1/2, k) = s$, $(i, j, k - 1/2) = a$ and $(i, j, k + 1/2) = b$. For

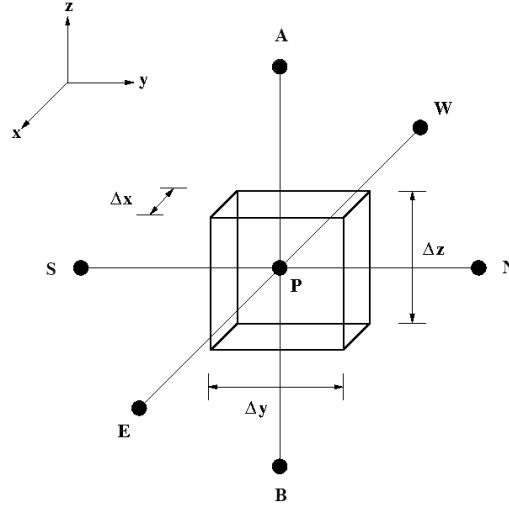


Figure 1. A three-dimensional finite volume

a computational mesh in which the center of cell P has coordinates (i, j, k) , its neighboring nodes will have coordinates $(i - 1, j, k) = W$, $(i + 1, j, k) = E$, $(i, j + 1, k) = N$, $(i, j - 1, k) = S$, $(i, j, k - 1) = B$, and $(i, j, k + 1) = A$. Therefore, after integration in space and time, we use a conservative expansion for the accumulation terms [6] and obtain the final discretized form of the governing equations [7]

$$\Delta (T_g \Delta p_g)_P^{n+1} - \Delta \left(T_g \frac{\rho_{gsc} g}{B_g} \Delta D \right)_P^{n+1} = C_{gp} \Delta t p_g + C_{ap} \Delta t p_g + C_{gs} \Delta t S_w - q_{scgP}^{n+1} \quad (13)$$

$$\Delta (T_w \Delta p_g)_P^{n+1} - \Delta (T_w \Delta p_c)_P^{n+1} - \Delta \left(T_w \frac{\rho_{wsc} g}{B_w} \Delta D \right)_P^{n+1} = C_{wp} \Delta t p_g + C_{ws} \Delta t S_w - q_{scwP}^{n+1}, \quad (14)$$

where, considering ρ_s constant [4],

$$C_{gp} = \frac{V_P}{\Delta t} \left\{ \left[\phi_P^{n+1} \left(\frac{1}{B_g} \right)'_P + \frac{\phi'_P}{B_{gP}^n} \right] (1 - S_{wP}^n) \right\}, \quad C_{gs} = -\frac{V_P}{\Delta t} \left(\frac{\phi_P^{n+1}}{B_{gP}^{n+1}} \right), \quad (15)$$

$$C_{ap} = \frac{V_P \rho_s}{\Delta t} \left[V_{adsP}^{n+1} \left(\frac{1}{B_g} \right)'_P + \frac{V'_{adsP}}{B_{gP}^n} \right], \quad C_{ws} = \frac{V_P}{\Delta t} \left(\frac{\phi_P^{n+1}}{B_{wP}^{n+1}} \right), \quad (16)$$

$$C_{wp} = \frac{V_P}{\Delta t} \left\{ \left[\phi_P^{n+1} \left(\frac{1}{B_w} \right)'_P + \frac{\phi'_P}{B_{wP}^n} \right] S_{wP}^n \right\}, \quad (17)$$

and we introduced the operators $\Delta (\xi \Delta \eta)_P$ and $\Delta_t \varphi$ defined by [6]

$$\Delta (\xi \Delta \eta)_P \equiv \xi_{x_w} (\eta_W - \eta_P) + \xi_{x_e} (\eta_E - \eta_P) + \xi_{y_n} (\eta_N - \eta_P) + \xi_{y_s} (\eta_S - \eta_P) + \xi_{z_a} (\eta_T - \eta_P) + \xi_{z_b} (\eta_B - \eta_P) \quad (18)$$

$$\Delta_t \varphi \equiv \varphi_P^{n+1} - \varphi_P^n \quad (19)$$

in addition to transmissibilities (T_α). For example, in the x -axis, they are defined as

$$T_{gx_f} \equiv \left(\frac{k_x A_x k_{rg}}{\mu_g B_g \Delta x} \right)_f \quad (20)$$

for $f = w$ or $f = e$, with similar expressions for the water phase equation. We obtain analogous results for the y - and z -directions. The interface properties, derivatives, and time steps follow the discussions by Freitas [7].

We apply a Picard-Newton method [8] to determine gas pressure and water saturation. The main idea behind this formulation is that although the individual transmissibilities of each phase vary highly with the saturation of the wet phase (water), the sum of the two remains approximately constant over many time steps. As a result, the pressure field remains stable, even though the saturation of the wet phase can vary greatly.

Thus, Eqs. (13) and (14) are combined in order to eliminate the presence of water saturation evaluated at $n + 1$, with the non-linear coefficients evaluated by applying the method of Picard. From this stage, we obtain a system of equations for the pressure of the gas phase [8]. On the other hand, we use linearization via the Newton-Raphson Method to solve Eq. (14), with the derivatives evaluated numerically, and we obtain a system of equations in terms of the saturation of the water phase [8]. An iterative process occurs to update the non-linear coefficients depending on the pressure values of the gas phase and saturation values of the water phase. The reader can find more information about the solution process in Freitas [7], including the application of Krylov subspace solvers and preconditioners.

4 Numerical results

Here, we present the results obtained for a two-phase water-gas flow, including the effects of adsorption, stress correction, and slippage. We indicate the different cases corresponding to our simulations as Case 1: Darcy flow without adsorption; Case 2: non-Darcy flow including stress correction, slippage, and adsorption; Case 3: Darcy flow with adsorption; Case 4: non-Darcy flow with slippage; and Case 5: non-Darcy flow with stress correction. On the other hand, the parameters set for the reference case are in Table 1 (the complete parameters set containing general data for gas-water flow simulations can be found in Freitas [7], including the well-reservoir coupling technique adopted).

Parameters	Value	Unit
Initial Reservoir pressure, P_0	4×10^3	psi
Pressure in standard condition, p_{sc}	14.696	psi
Temperature in standard condition, T_{sc}	519.67	R
Reservoir temperature, T	609.67	R
Rock compressibility, c_ϕ	4×10^{-6}	psi ⁻¹
Water Compressibility, c_w	1×10^{-5}	psi ⁻¹
Porosity, ϕ	0.07	–
Permeability, k	1×10^{-7}	Darcy
Initial water saturation, S_{w0}	0.20	–
Reservoir lengths in x -direction and in y -direction, L	1,000	ft
Length in z -direction, L_z	180	ft
Wellbore length, L_w	500	ft
Wellbore radius, r_w	0.1875	ft
Wellbore pressure, p_{wf}	2,000	psi
Langmuir pressure, p_L	1,300	psi
Langmuir volume, V_L	0.05	scf/lbm
Bulk density, ρ_s	150	lbm/ft ³
Stress correction rate, γ	1×10^{-4}	psi ⁻¹
Klinkenberg factor, b	1,000	psi

Table 1. Parameters for the reference case

For all simulations, the graphs show the curves for production rate (Q_g , downward curves) and accumulated production (V_a , upward curves), considering a horizontal well parallel to x -direction and placed at 25 ft far from the upper boundary, while the gas-cap zone limit is 90 ft far from the upper boundary.

First of all, we carried out a mesh convergence study, refining the spatial grid (Table 2), showing results in Fig. 2a, considering Case 1. As we refine the meshes, the flow rate and accumulated production curves become increasingly closer, so we chose Mesh 4 to perform the other simulations. Although the curves corresponding to Meshes 3 and 4 are very close (except for the first time steps when calculating the instantaneous flow into the region of the most significant influence of the numerical storage arising from the adopted well-reservoir coupling technique), they did not overlap.

Mesh	1	2	3	4
n_x	64	128	256	512
n_y	65	129	257	513
n_z	22	42	82	162

Table 2. Grids for refinement study

A comparison between Cases 1 and 2 is presented in Fig. 2b. It is possible to observe that the production flow and accumulated production are higher in Case 2, so that for the simulation parameters considered, the positive impacts of slippage, increasing the values of k_{ag} and of adsorption, increasing the volume of gas available in the system, overlapped the negative effect of stress correction, which reduces the gas apparent permeability due to reduced pressure in the producing region.

We compare, in Fig. 3a, the curves obtained for Cases 1, 2, 3, 4 and 5. From the analysis of the results, we noticed that the effects of slip and gas adsorption favor the increase in production, leading to higher recovered values than those obtained when the classical Darcy law is valid and/or when there is no adsorption. In Figs. 3b to 4b, we can find the results of the simulations for Case 2, in which we consider all incorporated physical effects simultaneously.

We see the respective curves determined from the variation of the Langmuir volume in Fig. 3b. As is physically expected, for higher values of V_L , we have higher amounts of adsorbed gas, leading to higher values of flow rate and accumulated production as the reservoir pressure declines over time. Next, we obtained the results by varying the parameter b (see Fig. 4a). The higher its value, the higher the gas slippage effect. This phenomenon favors gas flow, as there will be an increase in apparent permeability, thus leading to higher values of instantaneous flow rate and accumulated production.

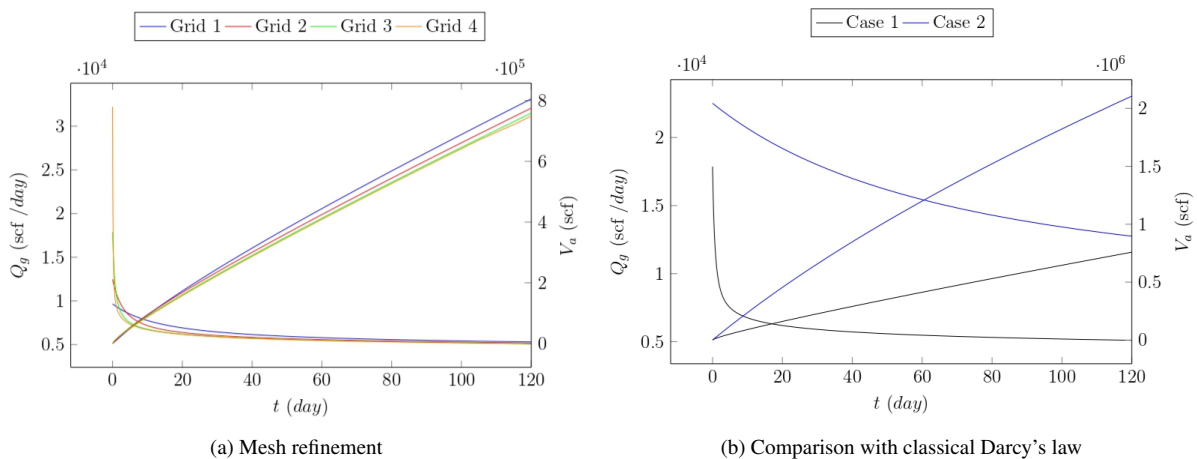


Figure 2. Production flow rate and accumulated production of gas as a function of time

Finally, in the case of the variation of γ , its higher values imply a reduction in the apparent gas permeability when there is a reduction in pressure in the porous medium (which is the situation studied), reducing the production

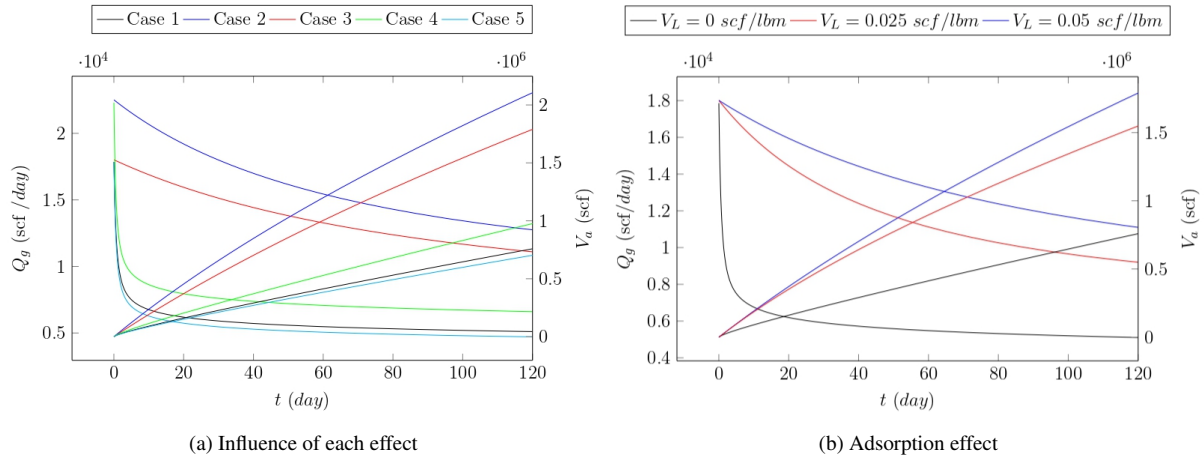


Figure 3. Production flow rate and accumulated production of gas as a function of time

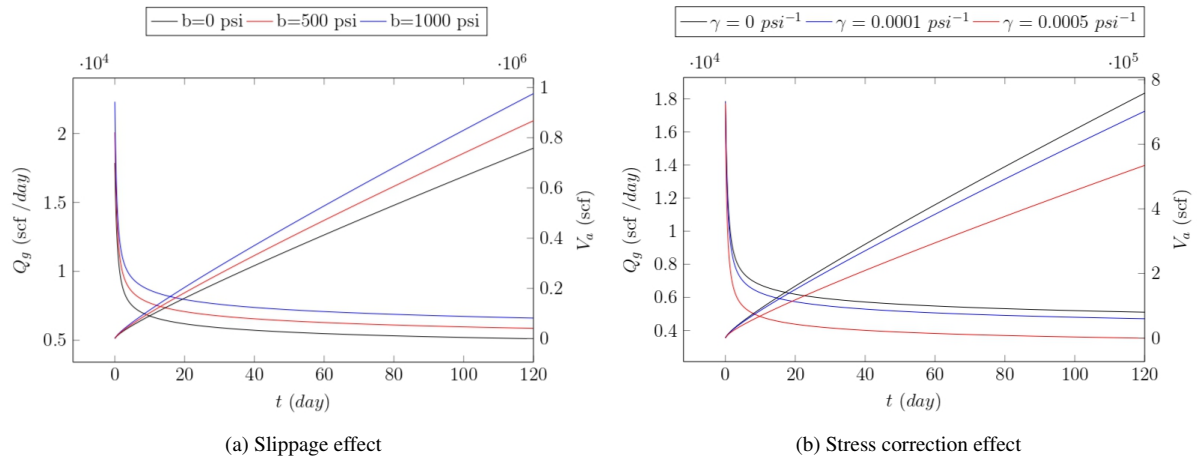


Figure 4. Production flow rate and accumulated production of gas as a function of time

flow rate and, therefore, consequently, accumulated production. We present the curves of these tests in Fig. 4b.

5 Conclusions

After carrying out the implementations and numerical simulations, we concluded that we captured the expected behaviors, considering the type of flow studied (in the future, we will have to accomplish a quantitative verification). Therefore, we understand that the formulation based on the Picard-Newton method was successful.

We also understand that the simulations undertaken in this work are relevant to implementing the best operating strategies. The differences found in accumulated production values, even for a short production time, such as the one studied here, indicated that an inappropriate model leads to non-negligible errors when making predictions aimed at realistic cases, remembering that production in a field occurs for decades.

Acknowledgements. This study was financed in part by the Coordenação de Aperfeiçoamento de Pessoal de Nível Superior - Brasil (CAPES) - Finance Code 001.

Authorship statement. The authors hereby confirm that they are the sole liable persons responsible for the authorship of this work, and that all material that has been herein included as part of the present paper is either the property (and authorship) of the authors, or has the permission of the owners to be included here.

References

- [1] M. Al-Twajjri, Z. Xia, W. Yu, L. Qu, Y. Hu, Y. Xu, and K. Sepehrnoori. Numerical study of complex fracture geometry effect on two-phase performance of shale-gas wells using the fast edfm method. *Journal of Petroleum Science and Engineering*, vol. 164, pp. 603–622, 2018.
- [2] Y. Xu, G. Sheng, H. Zhao, Y. Hui, Y. Zhou, J. Ma, X. Rao, X. Zhong, and J. Gong. A new approach for gas-water flow simulation in multi-fractured horizontal wells of shale gas reservoirs. *Journal of Petroleum Science and Engineering*, vol. 199, pp. 108292, 2021.
- [3] Y. He, J. Wang, X. Huang, Y. Du, X. Li, W. Zha, and D. Li. Investigation of low water recovery based on gas-water two-phase low-velocity non-darcy flow model for hydraulically fractured horizontal wells in shale. *Petroleum*, vol. 9, n. 3, pp. 364–372, 2023.
- [4] Y. Zhang and D. Yang. Modeling two-phase flow behaviour in a shale gas reservoir with complex fracture networks and flow dynamics. *Gas Science and Engineering*, vol. 119, pp. 205112, 2023.
- [5] R.-H. Zhang, L.-H. Zhang, H.-Y. Tang, S.-N. Chen, Y.-L. Zhao, J.-F. Wu, and K.-R. Wang. A simulator for production prediction of multistage fractured horizontal well in shale gas reservoir considering complex fracture geometry. *Journal of Natural Gas Science and Engineering*, vol. 67, pp. 14–29, 2019.
- [6] T. Ertekin, J. H. Abou-Kassem, and G. R. King. *Basic Applied Reservoir Simulation*. SPE Textbook Series 7. Society of Petroleum Engineers, Richardson, 2001.
- [7] M. M. Freitas. *Estudo Comparativo das Estratégias de Solução Numérica para Escoamentos Bifásicos em Reservatórios de Petróleo*. PhD thesis, Universidade do Estado do Rio de Janeiro, 2017.
- [8] M. M. Freitas, G. Souza, and H. P. Amaral Souto. A Picard-Newton approach for simulating two-phase flow in petroleum reservoirs. *International Journal of Advanced Engineering Research and Science*, vol. 7, pp. 428–457, 2020.